Inorganic Chemistry

Article

pubs.acs.org/IC

Crystal-Chemistry Guidelines for Noncentrosymmetric A_2BO_4 Ruddlesden–Popper Oxides

Prasanna V. Balachandran, Danilo Puggioni, and James M. Rondinelli*

Department of Materials Science & Engineering, Drexel University, Philadelphia, Pennsylvania 19104, United States

Supporting Information

ABSTRACT: Noncentrosymmetric (NCS) phases are seldom seen in layered A_2BO_4 Ruddlesden–Popper (214 RP) oxides. In this work, we uncover the underlying crystallographic symmetry restrictions that enforce the spatial parity operation of inversion and then subsequently show how to lift them to achieve NCS structures. Simple octahedral distortions alone, while impacting the electronic and magnetic properties, are insufficient. We show using group theory that the condensation of *two* distortion modes, which describe suitable symmetry unique octahedral distortions or a combination of a single octahedral distortion with a "compositional" A or B cation ordering mode, is able to transform the centrosymmetric aristotype into a NCS structure. With these symmetry guidelines, we formulate a data-driven model founded on Bayesian inference that allows us to rationally search for combinations of A- and B-site elements satisfying the inversion symmetry lifting criterion. We describe the general methodology and apply it to 214 iridates with A^{2+} cations, identifying RP-structured Ca_2IrO_4 as a potential NCS oxide, which we evaluate with density functional theory. We find a strong energetic competition between two closely related polar and nonpolar low-energy crystal structures in Ca_2IrO_4 and suggest pathways to stabilize the NCS structure.

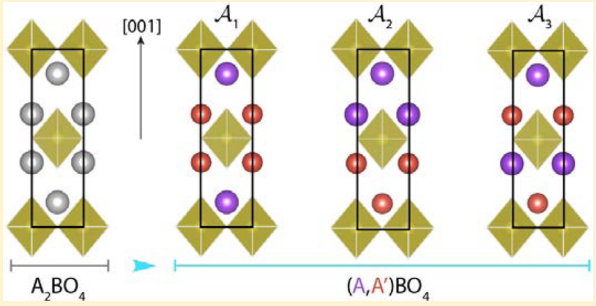

Noncentrosymmetric (NCS) solids lack an inversion center. In crystalline materials, the atomic arrangements that remove inversion symmetry[1] enable a number of technologically relevant macroscopic properties, including ferroelectricity, piezoelectricity, second-harmonic generation, and optical gyrotropy.[2] Medical imaging technologies and optical networks demand such high-performing inorganic materials with acentric properties; however, due to the overwhelmingly large chemical and structural phase space, a thorough exploration in search of new NCS materials for such applications *sans* design guidelines can be a formidable task.

Recently, this discovery process has been accelerated by applied theoretical crystallography,[3,4] where the objective is transformed into (i) identifying suitable topologies, approximate geometric arrangements of structural building units, that lift inversion symmetry, hence giving rise to NCS crystal structures, and then (ii) searching for microscopic mechanisms and external conditions to energetically stabilize those geometries. Such information may guide experimental explorations, whereby the synthetic efforts are focused on the theory-informed *and* more manageable structural data set.

Theoretical crystallography studies of this type have been extensively applied to the perovskite ABO_3 oxides in search of symmetry rules that impose constraints on the operation of inversion.[4−9] The guidelines result by considering how changes in point group and translation symmetry occur within a centrosymmetric (CS) space group of parent ABO_3 ($Pm\bar{3}m$) by adding either polar or nonpolar atomic displacements patterns, which transform as irreducible representations (irreps) of the parent phase at various high-symmetry points in the reciprocal k-space to form hettotypes.

While cooperative first-order Jahn–Teller distortions or octahedral rotations maintain the centricity of the perovskite structure,[3] recently applied group theoretical arguments have shown that the combination of cation ordering and octahedral rotations are sufficient to inversion symmetry in ordered $(A,A')B_2O_6$ perovskites without acentric atomic displacements.[4−10] Our interest in $(ABO_3)_{n=1}/(AO)$ Ruddlesden–Popper (214, RP) compounds stems from their layered two-dimensional (2D) topology.[11] The RP crystal structure may be derived from the perovskite structure by considering variations in layers of ABO_3 perovskite blocks stacked along the [001] direction with an extra sheet of an AO rocksalt layer interleaved every n layers (Figure 1). The reduced dimensionality derives from the stacking sequence of two disconnected BO_6 layers of octahedra along [001]. Yet, the layering maintains the *centricity* of the aristotype phase with space group symmetry $I4/mmm$. Nonetheless, the geometry imposes severe constraints on the nearest-neighbor interactions,[12] promoting anisotropy in the structure-derived electronic, transport, and magnetic properties, which contrasts sharply with their 3D perovskite analogues.[13,14]

Interestingly, our survey of reported crystal structures and chemistries for 214 RP oxides reveals that NCS structures are exceedingly rare (Figure 2). One of the reasons behind this

Received: September 8, 2013
Published: December 10, 2013

 © 2013 American Chemical Society

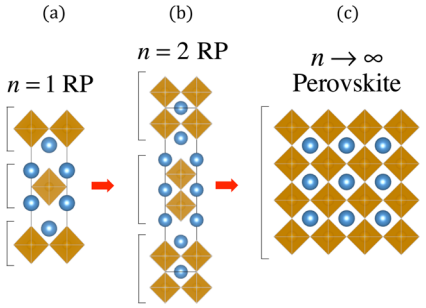

Figure 1. Relationship between octahedral connectivity of Ruddlesden–Popper phases $(ABO_3)_n/(AO)$ with different dimensionality (n) and the perovskite structure. (a) The n = 1 RP phase has a single layer of octahedra that are connected in two-dimensions, shown in brackets, whereas there is no connectivity in the third dimension. (b) The n = 2 RP phase contains two layers of octahedra connected in 3D, but beyond which, there is no further connection between perovskite-like layers. (c) The limit of $n\rightarrow\infty$ recovers the perovskite structure with complete 3D BO_6 connectivity.

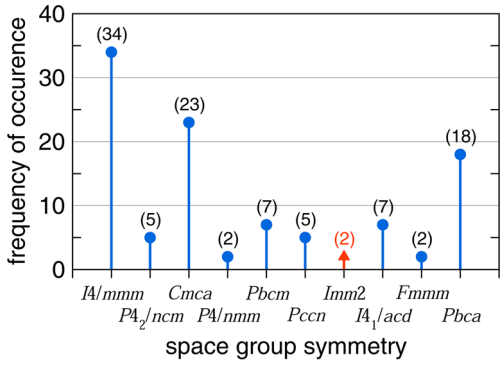

Figure 2. Frequency of occurrence of 214 RP oxides distributed among the crystallographic space groups. Our survey resulted in a total of 105 phases, which we note represents only a small fraction of the overall combinations of hypothetically feasible chemistries. Except two NCS compounds (space group, *Imm*2), Pb_2TiO_4 and $La_2Sr_2LiRuO_8$ (triangle, red), there are no other reports of NCS phases in 214 RP oxides.

paucity of NCS structures in 214 (n = 1) RP oxides, even when the octahedral site is occupied by second-order Jahn–Teller (SOJT) active cations such as Ti^{4+}, is attributed to the *layered* RP topology.[15] The disconnected TiO_6 octhaedral layers in Sr_2TiO_4 destroy the coherency required for cooperative off-centering displacements.[16] On the other hand, when the Sr A-site cation is replaced by the stereochemically active Pb^{2+} cation, a stable NCS polar space group *Imm*2 is predicted for Pb_2TiO_4 at the density functional theory (DFT) level even for the n = 1 with broken Ti–O–Ti chains;[17] albeit Pb_2TiO_4 has not yet been successfully synthesized. The only known polar n = 1 RP oxide that has been experimentally synthesized is the A- and B-site ordered $(La_2Sr_2)(LiRu)O_8$ compound, which is reported in the NCS *Imm*2 space group.[18] While the origin of ferroelectricity in Pb_2TiO_4 has been attributed to the stereochemical and SOJT activity of Pb^{2+} and Ti^{4+} cations, respectively, *cation ordering* on the A-site is crucial to removing inversion symmetry in $La_2Sr_2LiRuO_8$. Besides polar Pb_2TiO_4 and $La_2Sr_2LiRuO_8$, Ca_2MnO_4 is another example where experimental data indicate a possible polar structure. The coexistence of centrosymmetric and noncentrosymmetric phases within the same ceramic matrix,[19] however, make identification of the ground state ambiguous. Most researchers assign Ca_2MnO_4 to a centrosymmetric space group ($I4_1/acd$).[20]

Motivated by our own earlier studies on inversion symmetry breaking in 3D perovskite oxides and this scarcity of NCS 214 RP oxides, we report here a group theoretical (GT) analysis of the 214 RP structure with an emphasis on uncovering whether the interplay of cooperative atomic displacements, mainly structural distortions to the BO_6 units and/or cation ordering, gives way to NCS phases. We show that the coupling of two "distortion modes" is a necessary condition to lift inversion symmetry in 214 RP oxides in the absence of second-order Jahn–Teller cations. Data-mining methods establish a quantitative linkage between structural distortions and specific chemical elements in the crystal structure by exploiting our GT results with available experimental structural data. A probabilistic model, whose foundation lies in the Bayesian inference, is constructed to estimate the posterior probability of realizing such distortions given a particular chemical species. We then describe how to search for combinations of A- and B-site atoms that satisfy the multiple distortion criterion for lifting inversion symmetry. This protocol identifies Ca_2IrO_4 as a potential NCS oxide. The prediction is tested at the density functional theory level by computing the relative energetic stabilities of *ten* different crystal symmetries, revealing RP-structured Ca_2IrO_4 is near a CS and NCS structural phase boundary.

APPROACH AND METHODS

Group Theory and Data Mining Methods. We study hypothetical structural phase transitions in 214 RP structures to understand how multiple distortions may drive transitions to crystal symmetries lacking inversion centers. We treat this as an inverse Landau problem,[21,22] where when given a high-symmetry structure H and a distorted low-symmetry structure L, which is a subgroup of H, the goal is to find the irreducible representations (irreps) of H and the corresponding order parameter directions (OPD) that determine the transition. We examine the group–subgroup relationships between crystal symmetries of compounds that are known to exist and enumerate the permitted space groups and OPD for *multiple distortions*. Although earlier studies examined the group–subgroup relationships in RP compounds,[23] none have investigated in detail A/A′ or B/B′ cation ordering, coupling between two or more octahedral distortions (tilt or Jahn–Teller modes), or coupling between octahedral distortions and cation order. In this context, we also focus on the physical displacements that occur across that transition, i.e., attempting to understand and predict chemistries conducive to producing structures without inversion symmetry.

Although group theory offers the required mathematical rigor to study the inverse Landau problem and has been successfully applied to describe $H\rightarrow L$ phase transitions for various crystal systems,[24,25] the derived guidelines instructing how to lift inversion symmetry remain strictly mathematical. When taken alone, they cannot make predictions of candidate chemistries for new NCS 214 RP oxides. We overcome this limitation by integrating the GT methods with data-mining approaches and DFT calculations. Details of the 214 RP oxide database construction and formulation of Bayes' rules are described further below.

The high-symmetry structure, H, is the aristotype $I4/mmm$ containing two formula units per unit cell and two disconnected layers of octahedra (Figure 1). The occupied Wyckoff positions are specified in Table 1. The low-symmetry structures, L, are the hettotypes (summarized in Figure 2). [The compositions and references for these phases are available in the Supporting Information.] We interpret the $H\rightarrow L$ transition as second-order, where the order parameters are normal modes of lattice vibration, atomic-site ordering, or strain that are readily identified by irreps and wavevectors at high-symmetry k-points in the Brillouin zone (BZ) of the aristotype (Table 2). We employ the group theoretical packages

dx.doi.org/10.1021/ic402283c | Inorg. Chem. 2014, 53, 336–348

Table 1. Occupied Wyckoff Positions and Site Symmetries for the A_2BO_4 Phase with $I4/mmm$ ($a = b < c$) Symmetry[a]

atom	Wyck. site	site symm.	x	y	z
A	4*e*	4*mm*	0	0	u
B	2*a*	4/*mmm*	0	0	0
O(1)	4*c*	*mmm*	1/2	0	0
O(2)	4*c*	*mmm*	0	0	v

[a]The positions u and v are free parameters allowed to vary within the space group.

Table 2. Wavevectors for Irreps in the High-Symmetry Points of the $I4/mmm$ BZ and the Volume Change Ω'/Ω due to Condensation of a Symmetry-Adapted Mode within That Star

k-point	wavevector	Ω'/Ω
Γ	(0,0,0)	1−2
X	(1/2),(1/2),0)	2
P	(1/2),(1/2),(1/2)	4
M	(1,1,1)	1

ISOTROPY[26] and ISODISTORT[25] to identify these irreps, which follow the Miller and Love convention[27] and the "2011 notation" of Stokes and Hatch.[28]

Electronic Structure Calculations. DFT calculations on Ca_2IrO_4 are performed using the projector-augmented wave (PAW) formalism as implemented in the Vienna *Ab initio* Simulation Package (VASP)[29,30] within the revised generalized gradient approximation for densely packed solids (PBEsol).[31] A 550 eV plane-wave cutoff was used, and k-space integrations were performed on a 7 × 7 × 3 Monkhorst-Pack mesh.[32] A Gaussian smearing width of 0.02 eV was used for the Brillouin zone integrations. In all structural configurations, ferromagnetic spin order was imposed on the Ir cations, and the lattice parameters and atomic coordinates fully relaxed to within a convergence tolerance of 0.1 meV/Å for forces and 10^{-8} eV for total energy. Although Ir belongs to the 5*d* transition-metal series, where we would expect weak correlations but strong spin−orbit (SO) coupling, we do not explicitly include SO interactions or enhanced electron−electron interactions.[33] From previous studies on iridates, we find that such corrections do not significantly alter the description of the crystalline structure,[34] which is the focus of the present work, whereas they do renormalize the electronic structure.

RESULTS AND DISCUSSION

Distortion Modes in Experimental 214 RP Oxides. Among the *nine* existing hettotypes (Figure 2), the centrosymmetric *Cmca* and *Pbca* occur most frequently. The issue of space-group frequencies has been studied before; see, for example, the review by Brock and Dunitz.[35] In particular, it was found that materials with inversion symmetry are strongly favored (undistorted phases), because they reduce the number of "like−like" interactions in the crystalline state. The hettotype distribution may be further subdivided into five distinct groups according to the micropscopic distortions present relative to $I4/mmm$: (a) octahedral tilt modes (*Cmca*, $P4_2/ncm$, *Pccn*, and $I4_1/acd$), (b) A/A′ cation ordering that may (not) include octahedral tilts ($P4/nmm$ and *Pbcm*), (c) Jahn−Teller and octahedral distortions (*Pbca*), (d) ferroelectric or polar distortions (*Imm*2), (e) combination of A and B cation ordering (*Imm*2), and (f) ferroelastic or nonzero strain components (*Fmmm*).

In 214 RP oxides, it suffices to capture the general trends appearing in Figure 2 by using the well-established empirical tolerance factor model (t)[36] and crystal packing arguments. Unlike the three-dimensional perovskites where $t = 1$ is indicative of an undistorted structure, in the $n = 1$ RP phases, the susceptibility to resist distortion exists over a much larger range. In other words, the stability field for the undistorted tetragonal structure is wider: $0.907 \leq t \leq 1$. Indeed, the stability criterion is satisfied by ∼30 of the known 214 RP oxides.[36]

One reason for the wider stability field when compared to perovskites may be ascribed to the rigidity of the intervening rock-salt layers.[37] When the size of the A cation is large relative to the B cation, the network of BO_6 octahedra is under tension. Tilting of the BO_6 unit is considered to be unfavorable, because it would require a shortening of the A−O bonds, whereas the $n = 1$ RP would instead prefer to lengthen the A−O bonds. This distortion is accommodated by increasing the interlayer AO separation, relieving the chemical pressure. As a result of the disconnected structure, the BO_6 octahedron may distort without tilting or further symmetry reduction.[36] Thus, the observation of certain distortions appearing more frequently relative to others may be understood to result from a complex interplay between chemistry, lattice stresses, and the topology of 214 RP structures, which we note merits further attention.

Figure 3 depicts the group−subgroup relationship between the aristotype and the experimentally observed hettotypes along

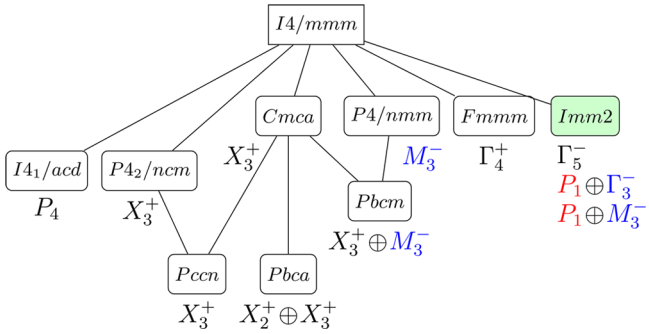

Figure 3. Group−subgroup relationships among the space groups of experimentally observed 214 RP oxides. Each structural distortion is associated with an irrep of the parent space group $I4/mmm$, with black color irreps indicating octahedral distortions, blue colors for A/A′ cation ordering, and red colors for B cation ordering. Coupled irreps are represented using the ⊕ symbol, and shaded space groups are NCS. This figure should be read in conjunction with Table 3, where the exact order parameter directions (OPD) are given. Lines connecting space groups indicate that phase transition is allowed to be continuous in Landau theory.

with the irrep labels accounting for the symmetry reduction. Table 3 summarizes the relevant order parameter directions (OPD) and physical distortion mode representations (MR). In the remainder of this section, we focus on observed octahedral tilt modes and cation ordering. Before proceeding, however, we make two notes: Some of the experimentally observed 214 RP oxides exhibit distortions described by irrep Γ_4^+, with OPD (η_1), which is associated with shear strain and the 214 structures may include the 2D irrep Γ_5^- with OPD (η_1,0) that produces *Imm*2 symmetry through a set of "proper" ferroelectric displacements. The *Imm*2 symmetry may also be stabilized in a 214 RP oxide owing to the coexistence of A and B cation ordering, whose action is described by the superposition of irreps $P_1 \oplus \Gamma_3^-$ or $P_1 \oplus M_3^-$.

Octahedral Tilt Modes. The octahedral tilt modes found in the experimental structures are associated with irreps of symmetry X_3^+, $X_2^+ \oplus X_3^+$, and P_4. The two-dimensional (2D)

dx.doi.org/10.1021/ic402283c | Inorg. Chem. 2014, 53, 336−348

Table 3. Experimental Distorted Structures Arising from Octahedral Tilting, Jahn-Teller Distortions, Cation Ordering, and the Interplay between Them[a]

irreps	OPD	lattice vectors	SG	MR
X_3^+	(η_1, η_1)	$\sqrt{2}a \times \sqrt{2}b \times c$	$P4_2/ncm$	rotations
	$(0, \eta_1)$	$\sqrt{2}a \times c \times \sqrt{2}b$	$Cmca$	rotations
	(η_1, η_2)	$\sqrt{2}a \times \sqrt{2}b \times c$	$Pccn$	rotations
P_4	$(\eta_1, -\eta_1)$	$\sqrt{2}a \times \sqrt{2}b \times 2c$	$I4_1/acd$	rotations
$X_2^+ \oplus X_3^+$	$(0, \eta_1; \eta_2, 0)$	$\sqrt{2}a \times c \times \sqrt{2}b$	$Pbca$	mixed rotations
M_3^-	(η_1)	$a \times b \times c$	$P4/nmm$	ACO
$X_3^+ \oplus M_3^-$	$(0, \eta_1; \eta_2)$	$c \times \sqrt{2}a \times \sqrt{2}b$	$Pbcm$	rotations + ACO
Γ_4^+	(η_1)	$\sqrt{2}a \times \sqrt{2}b \times c$	$Fmmm$	strain
Γ_5^-	$(\eta_1, 0)$	$b \times c \times a$	$Imm2$	polar displacement
$P_1 \oplus \Gamma_3^-$	$(\eta_1\eta_2; \eta_3)$	$\sqrt{2}a \times \sqrt{2}b \times 2c$	$Imm2$	BCO and ACO
$P_1 \oplus M_3^-$	$(\eta_1\eta_2; \eta_3)$	$\sqrt{2}a \times \sqrt{2}b \times 2c$	$Imm2$	ACO and BCO

[a]The corresponding irreps, order parameter direction (OPD), approximate unit cell parameters relative to the $I4/mmm$ tetragonal (T) aristotype ($a = b < c$), space group (SG), and mode representation (MR) of the distorted structure. Coupled irreps are represented using the ⊕ symbol. ACO and BCO stand for A-site and B-site cation ordering, respectively.

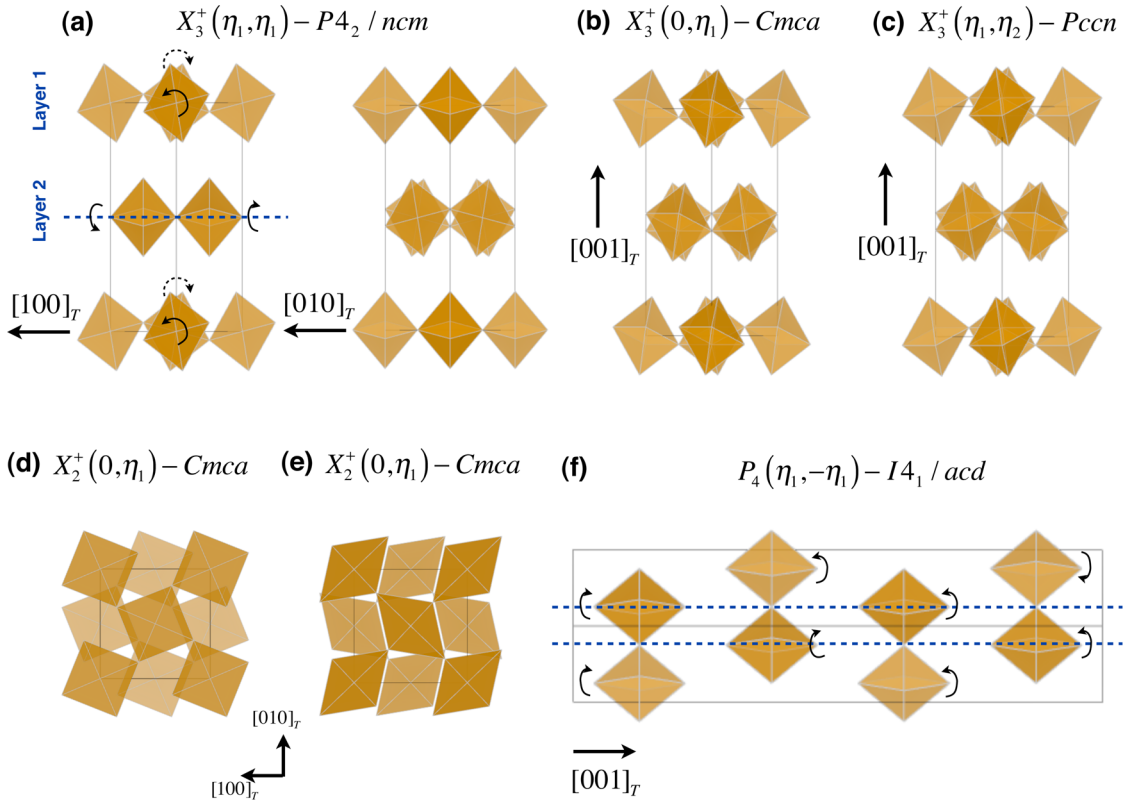

Figure 4. Illustration of octahedral tilt modes experimentally observed in 214 RP oxides. Irreps and the corresponding order parameters responsible for the primary distortion modes are also indicated. Oxygen atoms and cations are omitted for clarity.

irrep X_3^+ of $I4/mmm$ describes simple out-of-phase rotations of BO_6 octahedra, whereby the rotation axes and amplitude are specified by the OPD (Figure 4a–c). The general order parameter direction for X_3^+ is a two-component vector, $\boldsymbol{\eta} = (\eta_1, \eta_2)$, where each component η_i corresponds to the magnitude of tilt around the x and y axes of the parent tetragonal (T) $I4/mmm$ structure. For example, (η_1, η_1) and $(0, \eta_1)$ span one-dimensional subspaces containing one free parameter (η_1), whereas (η_1, η_2) spans a 2D subspace with two free parameters (η_1 and η_2). Correspondingly, their actions produce three distinct structures: $P4_2/ncm$ for (η_1, η_1), $Cmca$ for $(0, \eta_1)$, and $Pccn$ for (η_1, η_2) all with a mode representation of octahedral rotations.

The $I4/mmm \rightarrow P4_2/ncm$ and $I4/mmm \rightarrow Cmca$ transitions are allowed to be second-order, i.e., continuous as required by Landau theory, whereas $I4/mmm \rightarrow Pccn$ is not. The transition $I4/mmm \rightarrow Cmca \rightarrow Pccn$, however, through the $Cmca$ intermediate, is allowed to be second-order. The $P4_2/ncm$ structure preserves the tetragonal Bravais lattice, but the cell becomes primitive. The octahedra in Layer 1 are rotated out-of-phase about the $[100]_T$ direction, but in Layer 2, no rotations occur about the $[100]_T$ axis; instead, the out-of-phase BO_6 rotations in Layer 2 occur about the $[010]_T$ axis. Similarly, Layer 1 does not show any rotations about $[010]_T$ (Figure 4a); thus, the perovskite-like layers are related to each other by a 90° rotation.

dx.doi.org/10.1021/ic402283c | Inorg. Chem. 2014, 53, 336–348

In the *Cmca* and *Pccn* distorted structures, the Bravais lattice becomes orthorhombic. The BO_6 octahedra in Layers 1 and 2 are found to rotate out-of-phase along $[100]_T$ and $[010]_T$ axes. In the *Cmca* structure, the rotation angles are equal along both directions, whereas in the *Pccn* structure that requirement is lifted.

The direct sum $X_2^+ \oplus X_3^+$ spans a 2D order-parameter space $(0, \eta_1; \eta_2, 0)$ and transforms the parent tetragonal structure into an orthorhombic *Pbca* structure. In this coupled mode, the X_2^+ distortion is achieved *via* the action of a 2D parameter $(0, \eta_1)$, containing only one free parameter. It provides the parent oxygen atom (O1) with two displacive modes, in-phase octahedral rotation (Figure 4d) or a first-order Jahn–Teller distortion (Figure 4e). The latter mode manifests as the expansion and contraction of equatorial B–O bonds (in a two-in–two-out manner). The chemistry of the B cation, whether it is Jahn–Teller active or not, would determine the specific mode pattern. While the $I4/mmm \rightarrow Pbca$ transition is not continuous, $I4/mmm \rightarrow Cmca \rightarrow Pbca$ through the *Cmca* intermediate is continuous.

The 2D irrep P_4 corresponds to a set of cooperative out-of-phase octahedral rotations that differ from those described by either irreps X_2^+ or X_3^+. Figure 4f shows the complex tilt pattern, whereby neighboring layers of connected BO_6 octahedra rotate out-of-phase relative to each other with equal amplitude, i.e., OPD $(\eta_1, -\eta_1)$. To accommodate this tilt pattern, it requires a cell-doubling distortion along the long crystallographic axis and a 4_1 screw operation. Indeed, the crystal symmetry transforms to $I4_1/acd$, which is one of the more frequently observed structure types surveyed.

A/A′ Cation Order. Here, we consider the ordered substitution of cations on the A-site with chemically unique A′ cations as a *digital order–disorder transition*. The "disordered" configuration corresponds to the high-symmetry A_2BO_4 phase (despite possessing complete ordering and 100% occupancy of the *A*-site by a single cation), while the "ordered" configuration corresponds to an $(A,A')BO_4$ structure. In this picture, the irrep becomes a "composition mode," i.e., a scalar order parameter that fully characterizes the direction and arrangement of chemically unique A cations.

There are three simple A cation arrangements ($\mathcal{A}_i$, i = 1...3) that produce [001]-cation ordering in the $(A,A')BO_4$ 214 RP without changing the number of formula units per cell relative to the (unordered) A_2BO_4 aristotype (Figure 5). Since the composition is fixed, we decompose each cation-ordered structure into metal-oxide layers along the [001] direction to distinguish the various arrangements:

$$\mathcal{A}_1\text{: } [AO] - [A'O|BO_2|A'O] - [AO]$$

$$\mathcal{A}_2\text{: } [AO] - [AO|BO_2|A'O] - [A'O]$$

$$\mathcal{A}_3\text{: } [AO] - [A'O|BO_2|AO] - [A'O]$$

The key structural-chemistry feature being whether the chemically distinct AO or A′O layers are separated by a perovskite block or not.

Each cation-ordered structure in the absence of any atomic displacements leads to a crystallographic symmetry lowering relative to the unordered *I*4/*mmm* structure. The atomic structure parameters and site symmetries for the highest-symmetry $(A,A')BO_4$ compounds are enumerated in Table 4. The symmetry reduction for each cation ordering arrangement $\mathcal{A}_1$, $\mathcal{A}_2$, and $\mathcal{A}_3$ is described by composition modes which transform as irreps M_1^+, M_3^-, and Γ_3^- (Figure 5), respectively.

Arrangement $\mathcal{A}_1$, generated by irrep M_1^+ (Figure 5b), removes the body-center tetragonal lattice operations and renders the cell primitive. The cation order splits the formally equivalent A-site position into two symmetry unique sites (symmetry 4*mm*) and continues to permit freedom for the

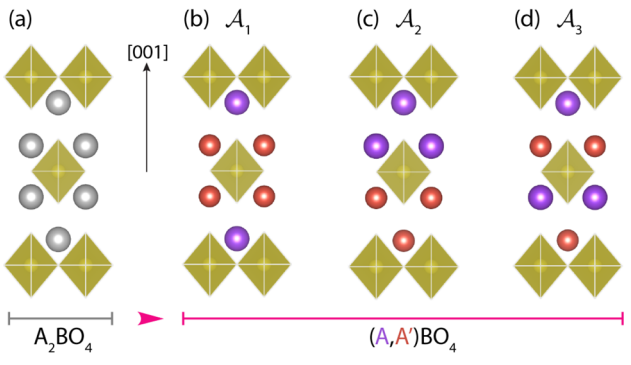

Figure 5. Structures of the simple $(A,A')BO_4$ cation ordering arrangements (b–d) along the [001] direction in the 214 RP phase shown relative to the A_2BO_4 aristotype with a single cation occupying the A-site (a).

Table 4. Crystallographic Data Including the Occupied Wyckoff Positions (Wyck. Site) for Each Cation Ordering Arrangement ($\mathcal{A}_i$) and Composition Mode Describing the Transition from A_2BO_4 to $(A,A')BO_4$[a]

$\mathcal{A}_1$ $[M_1^+ (\eta_1)]$			$a = b < c$		
*P*4/*mmm* (no. 123)			$\alpha = \beta = \gamma = 90°$		
atom	Wyck. site	site sym.	*x*	*y*	*z*
A	2*g*	4*mm*	0	0	*u*
A′	2*h*	4*mm*	1/2	1/2	*v*
B(1)	1*a*	4/*mmm*	0	0	0
B(2)	1*d*	4/*mmm*	1/2	1/2	1/2
O(1)	2*f*	*mmm*	0	1/2	0
O(2)	2*h*	4*mm*	1/2	1/2	*v*
O(3)	2*g*	4*mm*	0	0	*w*
O(4)	2*e*	*mmm*	0	1/2	1/2
$\mathcal{A}_2$ $[M_3^- (\eta_1)]$			$a = b < c$		
*P*4/*nmm* (no. 129)			$\alpha = \beta = \gamma = 90°$		
atom	Wyck. site	site sym.	*x*	*y*	*z*
A	2*c*	4*mm*	1/4	1/4	$1 - u$
A′	2*c*	4*mm*	1/4	1/4	$(1/2) + u$
B	2*c*	4*mm*	1/4	1/4	1/4
O(1)	4*f*	2*mm*	3/4	1/4	3/4
O(2)	2*c*	4*mm*	1/4	1/4	*v*
O(3)	2*c*	4*mm*	1/4	1/4	*w*
$\mathcal{A}_3$ $[\Gamma_3^- (\eta_1)]$			$a = b < c$		
*I*4*mm* (no. 107)			$\alpha = \beta = \gamma = 90°$		
atom	Wyck. site	site sym.	*x*	*y*	*z*
A	2*a*	4*mm*	0	0	$(1/2) - u$
A′	2*a*	4*mm*	0	0	$(1/2) + u$
B	2*a*	4*mm*	0	0	0
O(1)	2*a*	4*mm*	0	1/2	0
O(2)	2*a*	4*mm*	0	0	*v*
O(3)	2*a*	4*mm*	0	0	$1 - v$

[a]Atom positions are given relative to the ideal tetragonal symmetry; free positions are indicated by italic lowercase Roman letters.

dx.doi.org/10.1021/ic402283c | *Inorg. Chem.* 2014, 53, 336–348

cations' z positions. Interestingly, the A/A′ cation ordering indirectly splits the B cation sites into two orbits (simultaneously with the equatorial oxygen sites) and the remaining oxygen sites in the structure.

The second cation arrangement, described by irrep M_3^-, is antisymmetric with respect to the inversion (Figure 5c) and removes inversion in the site-symmetries of all occupied positions (Table 4). The A-site ordering A→A/A′ splits the A-site Wyckoff positions such that $4e$→$2c$/$2c$. The O(2) Wyckoff orbits split in the same manner. This in turn lowers the B-site symmetry to 4*mm*, without any splitting of its Wyckoff orbit as found in $\mathcal{A}_1$, corresponding to a *P*4/*nmm* structure. 214 RP oxides with arrangement $\mathcal{A}_2$ are experimentally known to exist, e.g., space groups *P*4/*nmm* and *Pbcm*.[38,39] In the case of *P*4/*nmm*, the octahedra are undistorted, whereas in *Pbcm* octahedral tilt modes associated with irrep X_3^+ with OPD (η_1,η_1) are involved.

The last cation order ($\mathcal{A}_3$) transforms as irrep Γ_3^- and maintains the body-centered tetragonal lattice, however, it globally lifts inversion symmetry to yield the polar space group *I*4*mm*. Interestingly, the $\mathcal{A}_3$ "bi-color" ordering in the 214 RP structures lifts inversion simply through the compositional ordering *and* the bidimensionality of the structure, which does not occur in 3D A/A′ ordered double perovskites.

We note that the irreps used to describe composition ordering may also capture the symmetry changes induced by displacive modes, i.e., describing collective atomic displacements, and may be present simultaneously or as secondary distortion modes in the transition connecting the aristotype to the hettotype. The *I*4/*mmm*→*P*4*mm* phase transition provides a good example of this behavior. The *I*4/*mmm*→*P*4*mm* transition can arise from the direct sum $\Gamma_3^-\oplus M_3^-\oplus M_1^+$ with the general OPD $(\eta_1; \eta_2; \eta_3)$ as shown in Figure 6. In this case,

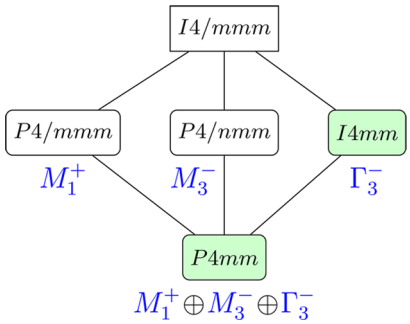

Figure 6. Group−subgroup relationships between CS and NCS (shaded) space groups arising from A/A′ cation ordering.

any two of the three irreps Γ_3^-, M_3^-, or M_1^+ could serve as the two active modes across the *I*4/*mmm*→*P*4*mm* phase transition. For example, $\mathcal{A}_1$ cation ordering (irrep M_1^+) may favor atomic distortions that transform like irrep M_3^-. These two "distortions" alone, $M_1^+\oplus M_3^-$, would account and produce a structure with *P*4*mm* symmetry, which then allows for additional (secondary) displacements with Γ_3^- symmetry.

B Cation Order. The B-site cation ordering found in experimental structures is associated with a 2D irrep of symmetry P_1 (Figure 7). There are three OPDs, $(\eta_1, -\eta_1)$, $(0, \eta_1)$, and (η_1, η_2), whose action would result in three different *centrosymmetric* space groups: *I*4$_1$/*amd*, *I*4/*mmm*, and $I\bar{4}m2$, respectively. Among the three OPDs, (η_1, η_2) is experimentally found[18] to exist in $La_2Sr_2LiRuO_8$, which orders

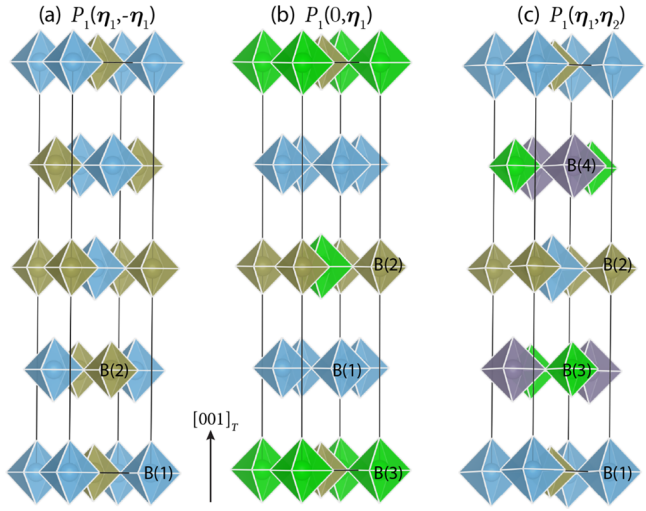

Figure 7. Structural variants available from B-cation order owing to the experimentally observed compositional order parameter P_1. The OPD directs the number of inequivalent B cations and the relative arrangement in the 214 RP structure.

the Li and Ru atoms in the arrangement depicted in Figure 7c. The main differences in the OPDs appear in the splitting of the B-site Wyckoff orbits. OPDs $(\eta_1, -\eta_1)$, $(0, \eta_1)$, and (η_1, η_2) split the B-site into two, three, and four unique Wyckoff sites, respectively, with a concomitant splitting of the A-site Wyckoff orbits induced by the B-cation order. Besides P_1, the 2D irrep X_1^+ would also result in B-site cation order. Since there are no experimental observations of B-cation order transforming as irrep X_1^+, we omit its discussion here. The reader is referred to the Supporting Information for more details about the crystallographic symmetries available from X_1^+.

Symmetry Consequences from Multiple Modes. We enumerate the changes in crystallographic symmetry from the combination of two or more octahedral distortions of the single experimentally observed modes or the combination of observed octahedral rotations with the discussed A/A′ cation order.

Coupled Octahedral Tilting. The group−subgroup relationships obtained by coupled multiple rotations are shown in Figure 8 and summarized in the first block of Table 5. We first

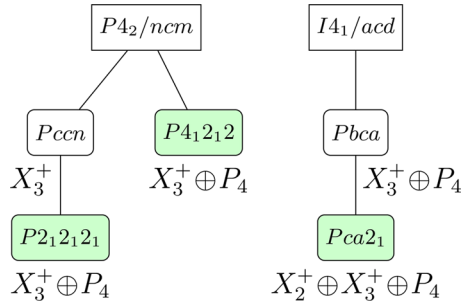

Figure 8. Group−subgroup relationships between CS and NCS (shaded) space groups arising from coupled BO_6 modes.

consider three tilt systems obtained by the direct sum, $X_3^+\oplus P_4$, which may be written as the superposition of tilt patterns given by the OPDs $(\eta_1, \eta_1; \eta_2, -\eta_2)$, $(0, \eta_1; \eta_2, -\eta_2)$, and $(\eta_1, \eta_2; \eta_3, -\eta_3)$. The corresponding crystal symmetries of the distorted phases are $P4_12_12$, *Pbca*, and $P2_12_12_1$, respectively, with $P4_12_12$ and $P2_12_12_1$ NCS and chiral (Figure 8).

dx.doi.org/10.1021/ic402283c | Inorg. Chem. 2014, 53, 336−348

Table 5. Irreps, Order Parameter Directions (OPD), Lattice Vectors ($a = b < c$), and Space Groups (SG) of Distorted Structures Arising from Coupled Rotational Modes, Neither Experimentally Observed nor Theoretically Predicted

irreps	OPD	lattice vectors	SG
$X_3^+ \oplus P_4$	$(\eta_1, \eta_1; \eta_2, -\eta_2)$	$\sqrt{2}a \times \sqrt{2}b \times 2c$	$P4_12_12$
	$(0, \eta_1; \eta_2, -\eta_2)$	$\sqrt{2}a \times 2c \times \sqrt{2}b$	$Pbca$
	$(\eta_1, \eta_2; \eta_3, -\eta_3)$	$\sqrt{2}a \times 2c \times \sqrt{2}b$	$P2_12_12_1$
$X_2^+ \oplus X_3^+ \oplus P_4$	$(0, \eta_1; \eta_2, 0; \eta_3, -\eta_3)$	$\sqrt{2}a \times 2c \times \sqrt{2}b$	$Pca2_1$
	$(0, \eta_1; \eta_2, \eta_3; \eta_4, -\eta_4)$	$2c \times \sqrt{2}b \times \sqrt{2}a$	$P2_1$
$X_3^+ \oplus \Gamma_3^-$	$(\eta_1, \eta_1; \eta_2)$	$\sqrt{2}b \times \sqrt{2}a \times c$	$P4_2cm$
	$(0, \eta_1; \eta_2)$	$\sqrt{2}a \times \sqrt{2}b \times c$	$Abm2$
	$(\eta_1, \eta_2; \eta_3)$	$\sqrt{2}b \times \sqrt{2}a \times c$	$Pcc2$
$X_2^+ \oplus X_3^+ \oplus \Gamma_3^-$	$(0, \eta_1; \eta_2, 0; \eta_3)$	$\sqrt{2}b \times \sqrt{2}a \times c$	$Pca2_1$
$P_4 \oplus \Gamma_3^-$	$(\eta_1, -\eta_1; \eta_2)$	$\sqrt{2}a \times \sqrt{2}b \times 2c$	$I4_1cd$
$X_3^+ \oplus M_3^-$	$(\eta_1, \eta_1; \eta_2)$	$\sqrt{2}b \times \sqrt{2}a \times c$	$P\bar{4}2_1m$
	$(\eta_1, \eta_2; \eta_3)$	$\sqrt{2}b \times \sqrt{2}a \times c$	$P2_12_12$
$X_2^+ \oplus X_3^+ \oplus M_3^-$	$(0, \eta_1; \eta_2, 0; \eta_3)$	$\sqrt{2}a \times 2c \times \sqrt{2}b$	$Pca2_1$
$P_4 \oplus M_3^-$	$(\eta_1, -\eta_1; \eta_2)$	$2c \times \sqrt{2}a \times \sqrt{2}b$	$Ibca$
$X_3^+ \oplus M_1^+$	$(\eta_1, \eta_1; \eta_2)$	$2a \times 2b \times c$	$Cmma$
	$(0, \eta_1; \eta_2)$	$\sqrt{2}a \times c \times \sqrt{2}b$	$Pmna$
	$(\eta_1, \eta_2; \eta_3)$	$\sqrt{2}a \times c \times 2b$	$P2/c$

We also considered tilt systems for the direct sums: $X_2^+ \oplus X_3^+$ and $X_2^+ \oplus X_3^+ \oplus P_4$. The superposition of tilt patterns associated with the direct sum, $X_2^+ \oplus X_3^+$, do not lift the inversion symmetry. However, the direct sum $X_2^+ \oplus X_3^+ \oplus P_4$ for the superposition of tilt patterns associated with order parameters $(0, \eta_1; \eta_2 0; \eta_3, -\eta_3)$ and $(0, \eta_1; \eta_2, \eta_3; \eta_4, -\eta_4)$ yield NCS space groups $Pca2_1$ and $P2_1$, respectively. Both $Pca2_1$ and $P2_1$ are polar yet are obtained in this case through the combination of two nonpolar octahedral rotation modes. These tilt modes, if stabilized in an actual 214 RP oxide, could potentially lead to "hybrid improper ferroelectricity" (HIF) in those oxides, where two or more nonpolar modes cooperatively lift inversion symmetry, permitting ionic displacements that produce a macroscopic electric polarization. $Ca_3Mn_2O_7$, which is a $n = 2$ RP oxide, fulfills these requirements,[40] although the specific modes slightly differ from those discussed here.

A/A′ Cation Order with Octahedral Tilting. The group−subgroup relationships obtained from direct sums of irreps associated with A/A′ cation order and octahedral rotation modes are summarized in Figure 9. The relevant OPDs are given in the second block of Table 5. First, we find that direct sums involving irrep Γ_3^- (arrangement $\mathcal{A}_3$) always results in NCS crystal structures.

Although irrep M_3^- (arrangement $\mathcal{A}_2$) did not lead to a NCS structure alone, we find that the direct sum $X_3^+ \oplus M_3^-$, which describes the superposition of tilt patterns with OPDs $(\eta_1, \eta_1; \eta_2)$ or $(\eta_1, \eta_2; \eta_3)$ produces structures with $P\bar{4}2_1m$ or $P2_12_12$ symmetries, respectively. In addition, the direct sum $X_2^+ \oplus X_3^+ \oplus M_3^-$ $(0, \eta_1; \eta_2, 0; \eta_3)$ also yields a NCS crystal structure ($Pca2_1$). Recall that the direct sum $X_2^+ \oplus X_3^+$ alone, i.e., without A cation ordering arrangement $\mathcal{A}_2$, for the order parameter directions $(0, \eta_1; \eta_2, 0)$ results only in a centrosymmetric $Pbca$ structure. Finally, no direct sum between rotations explored in this work and irrep M_1^+ (arrangement $\mathcal{A}_1$) alone would produce a NCS space group.

B-Cation Order with Octahedral Tilting and A-Cation Order. Although B-site ordering alone does not always lift inversion symmetry, many NCS structures may be obtained when it is coupled with symmetry specific tilting modes and A-site ordering. Table 6 enumerates the available space groups, and the corresponding group−subgroup diagram capturing the symmetry relationships is shown in Figure 10. The main result is that B-cation order, similar to the A-cation order, offers additional crystal engineering pathways to produce NCS structures.

Ramifications of the Group Theoretical Analysis. To summarize, we find many previously unexplored symmetry pathways through which the cooperative BO_6 geometric distortions may lift inversion symmetry without SOJT-active ions. First, there are a number of ways to couple two or more octahedral rotation modes alone without ordering multiple cations on the A- and B-sites to lift inversion symmetry. On the other hand, given two A cations, there exist one trivial ordering that does not change the cell volume (arrangement, $\mathcal{A}_3$, irrep Γ_3^-) and removes inversion solely through the composition ordering *sans* any distortions to the BO_6 units. Bicolor A cation order described by arrangement $\mathcal{A}_2$ (irrep M_3^-) will also remove inversion symmetry in the 214 structure when combined with suitable octahedral rotations. Similarly, B-cation order described by the experimentally observed compositional mode P_1 when combined with suitable octahedral rotations or A-cation order will also produce NCS structures.

Although these are seemingly simple structural rules involving A/A′ cation order, B cation order, and octahedral distortions, there are experimental challenges to achieve precise

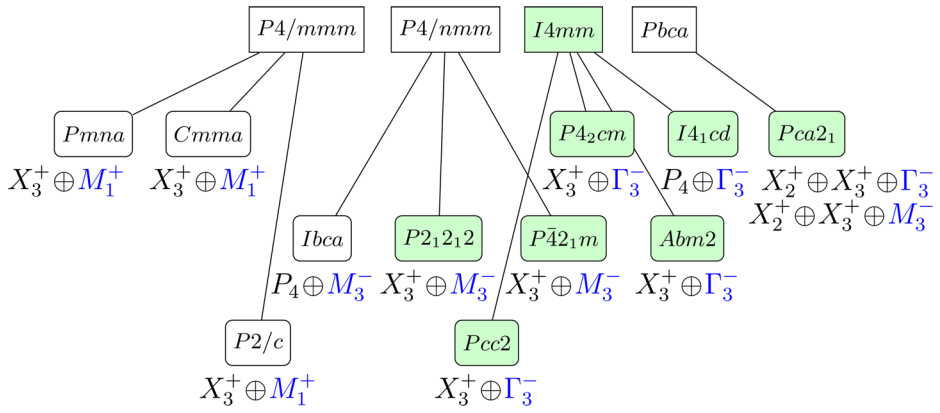

Figure 9. Group−subgroup relationships among the CS and NCS (shaded) space groups arising from the combination of octahedral rotation modes and A/A′ cation order.

dx.doi.org/10.1021/ic402283c | Inorg. Chem. 2014, 53, 336−348

Table 6. Irreps, Order Parameter Directions (OPD), Lattice Vectors ($a = b < c$), and Space Groups (SG) of Distorted Structures Arising from B-Site Ordering (P_1) and Coupled Modes

irreps	OPD	lattice vectors	SG
$P_1 \oplus X_3^+$	$(\eta_1, -\eta_1; 0, \eta_2)$	$\sqrt{2}a \times \sqrt{2}b \times 2c$	$Pnma$
	$(0, \eta_1; 0, \eta_2)$	$2c \times \sqrt{2}b \times \sqrt{2}a$	$Pnnm$
	$(\eta_1, \eta_2; 0, \eta_3)$	$\sqrt{2}a \times \sqrt{2}b \times 2c$	$Pmn2_1$
	$(\eta_1, -\eta_1; \eta_2, \eta_2)$	$\sqrt{2}a \times \sqrt{2}b \times 2c$	$P4_32_12$
	$(0, \eta_1; \eta_2, \eta_2)$	$2b \times 2a \times 2c$	$Cmca$
	$(\eta_1, \eta_2; \eta_3, \eta_3)$	$2a \times 2b \times 2c$	$C222_1$
	$(\eta_1, -\eta_1; \eta_2, \eta_3)$	$\sqrt{2}a \times 2c \times \sqrt{2}b$	$P2_12_12_1$
	$(0, \eta_1; \eta_2, \eta_3)$	$\sqrt{2}a \times 2c \times 2b$	$P2_1/c$
	$(\eta_1, \eta_2; \eta_3, \eta_4)$	$\sqrt{2}b \times 2c \times \sqrt{2}a$	$P2_1$
$P_1 \oplus P_4$	$(\eta_1, -\eta_1; \eta_2, -\eta_2)$	$\sqrt{2}a \times \sqrt{2}b \times 2c$	$I\bar{4}2d$
$P_1 \oplus X_2^+ \oplus X_3^+$	$(\eta_1, -\eta_1; 0, \eta_2; \eta_3, 0)$	$\sqrt{2}a \times 2c \times \sqrt{2}b$	$Pna2_1$
$P_1 \oplus \Gamma_3^-$	$(\eta_1, -\eta_1; \eta_2)$	$\sqrt{2}b \times \sqrt{2}a \times 2c$	$I4_1md$
	$(0, \eta_1; \eta_2)$	$\sqrt{2}b \times \sqrt{2}a \times 2c$	$I4mm$
	$(\eta_1, \eta_2; \eta_3)$	$\sqrt{2}b \times \sqrt{2}a \times 2c$	$Imm2$
$P_1 \oplus M_3^-$	$(\eta_1, -\eta_1; \eta_2)$	$\sqrt{2}b \times \sqrt{2}a \times 2c$	$Imma$
	$(0, \eta_1; \eta_2)$	$\sqrt{2}b \times \sqrt{2}a \times 2c$	$I4mm$
	$(\eta_1, \eta_2; \eta_3)$	$\sqrt{2}b \times \sqrt{2}a \times 2c$	$Imm2$
$P_1 \oplus M_1^+$	$(0, \eta_1; \eta_2)$	$\sqrt{2}b \times \sqrt{2}a \times 2c$	$I4/mmm$
	$(\eta_1, \eta_2; \eta_3)$	$\sqrt{2}b \times \sqrt{2}a \times 2c$	$I\bar{4}m2$

control over the cation arrangement and select chemistries that lead to the targeted low-symmetry geometries. Nonetheless, cation ordered RP oxides have been demonstrated using advanced solid-state chemistry methods[39] or thin film growth methods.[41] The principal challenge, therefore, is to rationally select the optimal chemical species; we address this next.

Bayes' Rules for NCS 214 RP Oxides. Having established the group−subgroup relationships and discovered potential symmetry pathways to tailor NCS phases, we seek to address the crystal chemistry question of whether those inversion symmetry breaking structural distortions could be realized in actual 214 RP oxide. Are there particular combinations of A and B cations that would induce the identified distortion modes to stabilize a NCS phase?

We begin to address this question by applying Bayes's rules, a Bayesian inference-based data-mining approach. Bayes' rule, also known as Bayes' theorem, is one of the well-known data-mining methods that combine prior experience, $p(\theta)$, with observed data or current evidence, $p(D)$, to make inference [*posterior*, $p(\theta|D)$] about the data.[42] Mathematically, the theorem is expressed as

$$p(\theta|D) = \frac{p(D|\theta)p(\theta)}{p(D)} \quad (1)$$

The prior, $p(\theta)$, is the strength of the belief in (structural distortions) θ *without* the data D about chemical elements and temperature. The *posterior*, $p(\theta|D)$, is the strength in the belief θ when data D about chemical elements and temperature *are given*.

In eq 1, $p(D|\theta)$ is usually referred to as the *likelihood*. The objective is to estimate the *posterior*, $p(\theta|D)$, from available structural data about A- and B-site elements (Figure 11), and temperature (Figure 12) to rapidly screen for A_2BO_4 chemical compositions and identify new and previously unexplored 214 RP chemistries conducive to the specified distortion patterns that lift inversion symmetry. One can then use a computational structure optimization method to compute the relative stabilities of the predicted phases.

The data-mining approach involves constructing a database of known compounds from which we extract "patterns" that give informative atomic site-chemistry and structural distortion relationships. We create a hybrid experimental and theoretical database consisting of chemical compositions of 214 RP oxides and their corresponding crystal structures (Table S1, Supporting Information) and encode the space groups using the previously determined irreps of $I4/mmm$. This allows us to use the group−subgroup diagrams with our data-driven structural chemistry models. For example, space group $I4_1/acd$ is encoded as a P_4 distortion. The Bayes' rules implemented in R[43] and our source code, along with the database, are available in the Supporting Information.

Before we demonstrate Bayes' rules, it should be noted that our data set (shown in Figure 2) presents critical nontrivial challenges due to its small sample size, unbalanced nature (not

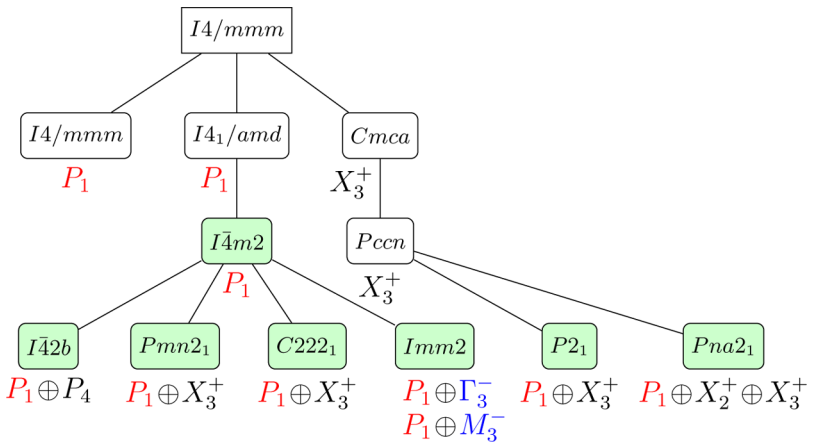

Figure 10. Group−subgroup relationships among the CS and NCS (shaded) space groups arising from the combination of B cation order, irrep $P_1(\eta_1, \eta_2)$ in red, with A/A′ cation order (irrep notations in blue) and octahedral rotation modes (irrep notations in black). Along the $I4/mmm \rightarrow I4/mmm$ path, there is no symmetry change; however, the cell size increases by a factor of 4 owing to the multiple B cations. Note that the group−subgroup relationships obtained from the superposition of OPDs $(\eta_1, -\eta_1)$ and $(0, \eta_1)$ for irrep P_1 with the A/A′ cation order and tilting modes are omitted, because they are not observed experimentally.

dx.doi.org/10.1021/ic402283c | Inorg. Chem. 2014, 53, 336−348

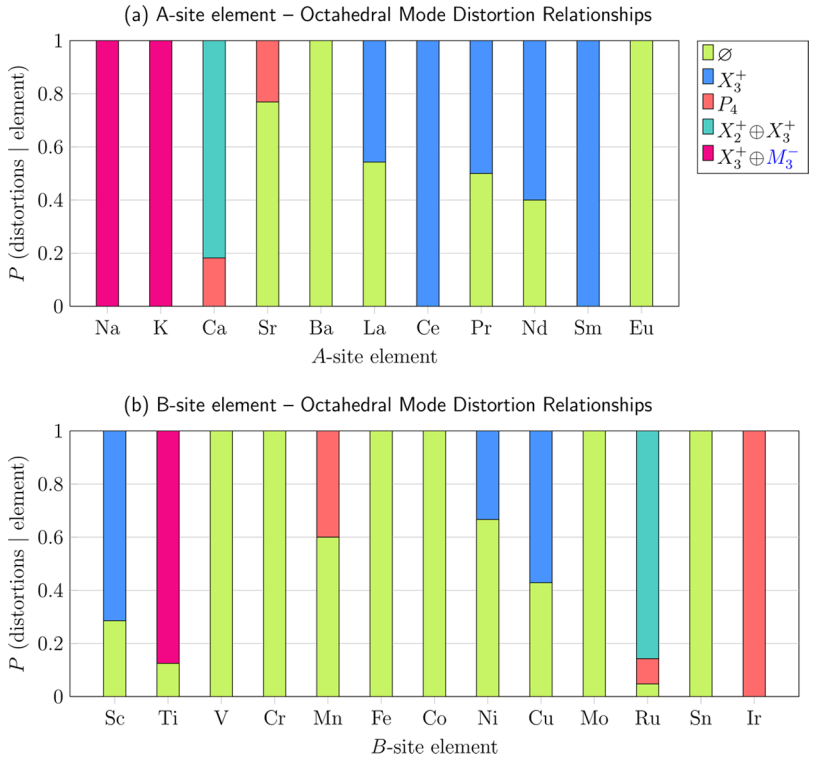

Figure 11. Posterior probabilities that a particular mode distortion, described by irreps of *I*4/*mmm* in 214 RP oxides, will be observed given a specific (a) A-site or (b) B-site element. These plots, when combined with a group−subgroup diagram, make it possible to rationally select A- and B-site elements conducive to specific structural distortions in 214 RP oxides. The ∅ indicates no tendency to octahedral distortions. The fact that we obtain nonzero probabilities for any two distortions given the same chemical species indicates that there is an interaction between A- and B-site elements and temperature, which we do not explicitly deconvolute.

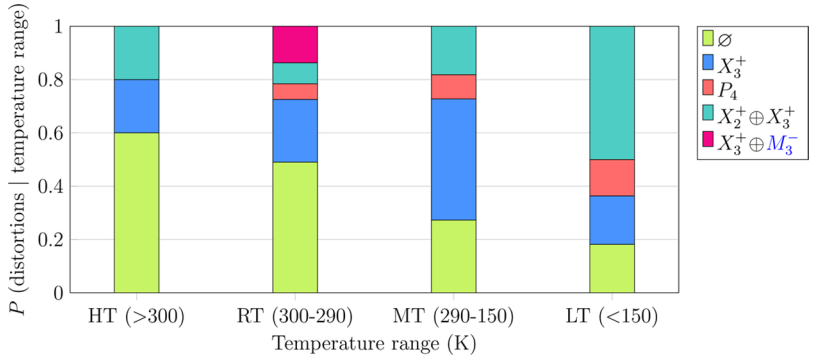

Figure 12. Estimated posteriors for the belief in structural distortions when data about temperature is given. The binning width determining the temperature range was chosen arbitrarily. The plot captures the relative tendency for various tilting instabilities as a function of temperature. As a general trend, the propensity for the BO_6 octahedra to distort increases with decreasing temperature.

all space groups are evenly distributed), and skewed chemistry distribution (some A- and B-site elements are studied more extensively than others). Therefore, to simplify our problem, we impose several "boundary conditions" that alleviate those challenges. First, we consider only a subset of compounds, whose frequency of occurrence is at least *seven* or more on the basis of our survey (Figure 2). This limits our search to *five* space groups (irreps): *I*4/*mmm* (undistorted, ∅), *Cmca* (X_3^+), $I4_1/acd$ (P_4), *Pbca* ($X_2^+ \oplus X_3^+$), and *Pbcm* ($X_3^+ \oplus M_3^-$). The constraint also reduces the number of compounds in our data set from 105 to 89 (88 of these structures are experimental and 1 is theoretical). Next, we treat A- and B-site elements as independent entities, i.e., we do not directly treat interactions between A, B, and substitutional elements. The oxidations states of the A- and B-site elements are also not explicitly considered. Finally, interactions between temperature and chemical elements are omitted.

As a result, we suggest that the insights gained from Bayes' rule analysis must be interpreted at a qualitative level. We also note that these simplifying assumptions could be potentially overcome by developing an alternative data set with a judicious choice of descriptors, where the oxidation states of the A- and B-site elements are considered, and by adapting advanced data-mining methods, e.g., Bayesian-belief networks, support-vector machines, random forests, and ensemble-decision trees (to name a few), which would treat the interaction between chemical elements and temperature on a more quantitative

dx.doi.org/10.1021/ic402283c | *Inorg. Chem.* 2014, 53, 336−348

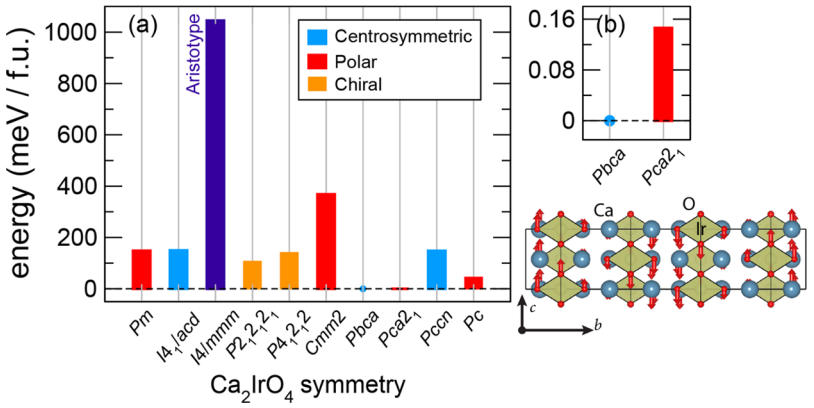

Figure 13. DFT computed energies for Ca_2IrO_4 with (a) different crystal symmetries in the 214 RP phase relative to the lowest energy *Pbca* phase. (b) There is close competition (near degeneracy) between a low-energy polar and centrosymmetric phase, which is distinguished from one another by a small buckling of O−Ir−O bond angles described by irrep Λ_5. Vectors indicate direction of atomic displacements from *Pbca* to the *Pca*2_1 structure. Note that the experimentally observed Ca_2IrO_4 structure with edge-shared octahedra is ∼57 meV lower in energy than the explored 214 RP structures, indicating nonequilibrium methods may be needed to stabilize the RP phases.

footing.[44−47] We are currently exploring the feasibility of these methods for a future publication.

How to Determine the Posterior, p(θ|D)? A simple worked example for estimating the posterior is discussed here. In our data set, there were a total of 11 unique A-site and 13 unique B-site elements. The probability of $X_2^+\oplus X_3^+$ distortion $p(\theta_{X_2^+\oplus X_3^+}) = 18/89 = 0.2$, and the probability of P_4 distortion $p(\theta_{P_4}) = 7/89 = 0.078$. There are 22 occurrences of 214 RP oxides with Ca in the A-site, obtained from the 18 occurrences with $X_2^+\oplus X_3^+$ distortion, 4 occurrences with P_4 distortion, and no occurrences with other types of distortions. The overall probability of finding Ca in the A-site is 22/89 = 0.247, i.e., $p(D_{Ca}) = 0.247$. The likelihood of finding Ca in the A-site given the $X_2^+\oplus X_3^+$ distortion is estimated as $p(D_{Ca}|\theta_{X_2^+\oplus X_3^+}) = 18/18 = 1$. Similarly, the likelihood of observing Ca element in the A-site given the P_4 distortion is estimated as $p(D_{Ca}|\theta_{P_4}) = 4/7 = 0.57$, and finally, the likelihood for any other distortion is zero. The posterior probabilities are obtained as follows:

$$p(\theta_{X_2^+\oplus X_3^+}|D_{Ca}) = \frac{1.0 \times 0.2}{0.247} = 0.81$$

$$p(\theta_{P_4}|D_{Ca}) = \frac{0.57 \times 0.078}{0.247} = 0.19$$

Bayes' rule capture one of the key physical features associated with Ca element in the A-site of the 214 oxides: Among the BO_6 octahedra tilts modes, there is a relatively stronger tendency for the coupled $X_2^+\oplus X_3^+$ rotation mode to occur than the P_4 tilt distortion. The propensity toward octahedral tilting could be rationalized on the basis of the relatively small size of Ca^{2+} in the 214 lattice: simple BO_6 octahedral tilts are more likely to occur so as to produce more favorable bond-valences for the cations.

Evaluation of Bayes' Rules. We provide a validation for our Bayes' rules using Ba_2IrO_4 RP phase as an example. We note that Ba_2IrO_4 was not included in our data set to determine the *posterior*. Recently, Okabe et al. successfully synthesized Ba_2IrO_4 using a high-pressure synthesis technique.[48] They determined the crystal structure of Ba_2IrO_4 to be *I*4/*mmm* at 293 K. From Figure 11, we learn that, when Ir atoms occupy the B-site, our estimated *posterior* probability for P_4 distortion is 1.0, which suggests that IrO_6 octahedra prefer to strongly distort with a tilt mode associated with irrep P_4 (Figure 4f). On the other hand, when Ba atoms occupy the A-site, our estimated *posterior* based on available data for an undistorted octahedra is 1.0; Ba suppresses the BO_6 octahedral rotations.

If we assume that the distortions are additive when we combine Ba and Ir to form the 214 RP structure, we would obtain two distinct possibilities: an undistorted Ba_2IrO_4 structure with space group *I*4/*mmm* or a distorted phase dominated by the P_4 rotation modes with *I*4$_1$/*acd* symmetry. The first scenario agrees with the experimental work of Okabe et al., giving confidence to our Bayes' rules. We note that, at low temperatures, however, Ba_2IrO_4 may adopt the distorted *I*4$_1$/*acd* structure. The rationale for this prediction comes from Figure 12, which captures the *posterior* probabilities for structural distortions as a function of temperature. We find that at lower temperatures the tendency for BO_6 octahedra to distort increases. The measurements by Okabe et al. fall in the "RT" (290−300 K) range; below that, however, the relative tendency for the P_4 BO_6 distortions *increases* in the MT and LT ranges, whereas the probability of 214 oxides with undistorted octahedra correspondingly *decreases*. We tested this hypothesis using zero-Kelvin DFT calculations, which reveal that the distorted *I*4$_1$/*acd* phase is indeed 25 meV/f.u. lower in energy relative to the undistorted *I*4/*mmm* phase. We are unaware of any temperature-dependent diffraction studies on Ba_2IrO_4 and suggest the experimental search for the predicted antiferrodistortive *I*4/*mmm*→*I*4$_1$/*acd* phase transition at low temperatures.[49]

Rational Search for NCS 214 RP Oxides. We now combine our estimated posteriors (Figure 11) with the group−subgroup diagram (Figure 6) to search for new NCS 214 RP oxide chemistries using coupled rotation modes alone. Which elements should we put on the A- and B-sites? As discussed, when Ca atoms occupy the A-site, two distortions are generally observed, $X_2^+\oplus X_3^+$ and P_4. When Ir occupies the B-site, our estimated *posterior* probability for P_4 distortion is 1.0, which suggests that IrO_6 prefer to distort with a complex tilt pattern about an axis of rotation along the doubled cell parameter (Figure 4f). When we combine these cations to form a "virtual" Ca_2IrO_4 RP oxide and under the assumption that the distortions are also additive, we obtain three possible direct sums, $X_2^+\oplus X_3^+$, $X_2^+\oplus X_3^+\oplus P_4$, and P_4, yielding space groups *Pbca*,

dx.doi.org/10.1021/ic402283c | *Inorg. Chem.* 2014, 53, 336−348

$Pca2_1$, and $I4_1/acd$, respectively. Of these combinations, only $Pca2_1$ is NCS.

Although previous experimental studies report the successful synthesis of divalent A-site 214 iridates, including Sr_2IrO_4, Ba_2IrO_4, and $Sr_{2-x}La_xIrO_4$,[48,50] Ca_2IrO_4 appears to be an exception. It does not form in the 214 RP phase[51] but rather prefers a structure with edge-shared rather than corner-shared octahedra in the RP topology. Nonetheless, we note that neither high-pressure synthesis nor epitaxial growth strategies have been explored to stabilize 214 Ca_2IrO_4 in the RP topology. Therefore, we continue with our theoretical study with an optimistic view that the Ca_2IrO_4 RP phase could be synthesized.

We compute the total energies of Ca_2IrO_4 in the *Pbca*, $Pca2_1$, $I4_1/acd$, and seven other symmetries using DFT (Figure 13). Centrosymmetric *Pbca* and NCS $Pca2_1$ are found to be the lowest energy structures among all the candidate geometries: the aristotype phase is found to be extremely high in energy, indicating if the RP phase is stable, the structure will be highly distorted. In addition, the nature of the distortions in Ca_2IrO_4 (coupled X_2^+, X_3^+, and a third mode described next) is significantly different from those found in the Mott insulator Sr_2IrO_4,[52] where the primary distortions are described by P_4 ($I4_1/acd$).

The primary order parameters[53] for the *I4/mmm*-to-*Pbca* transition are the octahedral tilt modes described by the coupled irreps $X_2^+ \oplus X_3^+$ (0, η_1; η_2, 0) (see Table 3). Symmetry-adapted mode decomposition analysis on the relaxed *Pbca* structure confirms the above-mentioned primary driving mechanisms. We identify the amplitudes for displacive modes described by X_2^+ and X_3^+ irreps to be 0.712 and 0.646 Å, respectively. Similar analysis of the fully relaxed $Pca2_1$ structure reveals that the ground state is obtained by the superposition of modes $X_2^+ \oplus X_3^+ \oplus \Lambda_5$, despite targeting $X_2^+ \oplus X_3^+ \oplus P_4$. Along the Λ_5 line of symmetry, there is an alternative pathway for the structure to distort into the $Pca2_1$ space group.

We propose the possible sequence of transitions in RP-structured Ca_2IrO_4 RP as $I4/mmm \rightarrow Pbca \rightarrow Pca2_1$, where *I4/mmm* is the high-temperature structure that transforms first to a distorted (centrosymmetric) *Pbca* phase and then potentially to a NCS $Pca2_1$ structure upon cooling and under suitable synthesis conditions. While the roles of X_2^+ and X_3^+ irreps in our optimized $Pca2_1$ structure are unambiguous, as their amplitudes are essentially unchanged from the *Pbca* geometry, the amplitude of Λ_5 [k = (0, 0, g), where $0 < g < (1/2)$] responsible for the symmetry reduction is quite small (0.001) Å. It displaces the oxygen atoms along the *c*-direction in a "zig-zag" fashion relative to *Pbca* and includes small Ca displacements (Figure 13b), which reduce the O−Ir−O bond angles by less than a degree.

This subtle structural difference is responsible for the strong energetic competition, i.e., we compute an energy difference per formula unit of ∼0.15 meV between the two phases (Figure 13b). As a result, we cannot conclusively identify the ground state as NCS with the present calculations; however, since epitaxial thin film strain−octahedral rotation coupling is strong in perovskite-like compounds,[54] we are hopeful that the polar $Pca2_1$ structure could be experimentally stabilized using strain engineering methods. Such approaches have been successful in stabilizing many nonequilibrium phases.[55] At present, we are exploring the strain and SOI effects in Ca_2IrO_4 with the goal of determining the optimal conditions to preferentially stabilize the $Pca2_1$ structure to guide subsequent experimentation.

SUMMARY

One of the major roadblocks in the discovery of NCS phases in 214 RP oxides has been the lack of symmetry governing design principles which incorporate chemical information to guide routes to lift inversion symmetry. In this work, we employed group theoretical methods to identify the structural distortions required to remove inversion from the aristotype phase. We found that simple octahedral tilting and Jahn−Teller ordering modes, although prevalent, are insufficient to meet this challenge alone. We discovered that, in combination with each other or with A or B cation ordering, however, it is possible to achieve a NCS crystal structure, provided the octahedral rotations or cation ordering can be energetically stabilized. The symmetry rules laid the foundation for establishing crystal-chemistry relationships needed for rational design of NCS 214 RP oxides. A data-driven probabilistic model was formulated using Bayes' theorem to provide an estimate of the probability of observing a particular distortion given a specific chemical element. We demonstrated how to integrate the group theoretical analysis with the probabilistic model and suggested Ca_2IrO_4 as a potential 214 RP oxide with a NCS structure. We evaluated the prediction using density functional theory calculations and found close competition between a polar and nonpolar phase with the targeted octahedral rotation modes.

ASSOCIATED CONTENT

Supporting Information

Additional tables, crystallographic data, and data-mining routines used in the calculations. This material is available free of charge via the Internet at http://pubs.acs.org/.

AUTHOR INFORMATION

Corresponding Author

*E-mail: jrondinelli@coe.drexel.edu.

Notes

The authors declare no competing financial interest.

ACKNOWLEDGMENTS

P.V.B. and J.M.R. would like to thank A. Bhattacharya, B. Nelson-Cheeseman, and H. Zhou for useful discussions. P.V.B. was supported by DARPA (Grant No. N66001-12-4224); J.M.R. and D.P. acknowledge support from ONR (N00014-11-1-0664) and ARO (W911NF-12-1-0133), respectively. DFT calculations were performed using DOD facilities supported by the HPCMP. The views, opinions, and/or findings reported here are solely those of the authors and do not represent any official views of the funding agencies.

REFERENCES

(1) The specific responses depend on the point group symmetry, i.e., polar, chiral, or both, whereby the absence of mirror operations or improper rotations, respectively, occurs.

(2) Halasyamani, P. S.; Poeppelmeier, K. R. *Chem. Mater.* **1998**, *10*, 2753−2769.

(3) (a) Stokes, H. T.; Kisi, E. H.; Hatch, D. M.; Howard, C. J. *Acta Crystallogr., Sect. B* **2002**, *58*, 934−938. (b) Abrahams, S. C. *Acta Crystallogr., Sect. B* **2003**, *59*, 541−556. (c) Abrahams, S. C. *Acta Crystallogr., Sect. B* **2006**, *62*, 26−41. (d) Bennett, J. W.; Garrity, K. F.; Rabe, K. M.; Vanderbilt, D. *Phys. Rev. Lett.* **2013**, *110*, 017603. (e) Bennett, J. W.; Rabe, K. M. *J. Solid State Chem.* **2012**, *195*, 21−31.

(4) Rondinelli, J. M.; Fennie, C. J. *Adv. Mater.* **2012**, *24*, 1961−1968.

(5) Mulder, A. T.; Benedek, N. A.; Rondinelli, J. M.; Fennie, C. J. *Adv. Funct. Mater.* **2013**, *23*, 4810−4820.
(6) Fukushima, T.; Stroppa, A.; Picozzi, S.; Pérez-Mato, J. M. *Phys. Chem. Chem. Phys.* **2011**, *13*, 12186−12190.
(7) Gou, G.; Rondinelli, J. M. *ArXiv e-prints* **2013**, *Cond-Mat*, Article ID: 1304.4911.
(8) Yamauchi, K. *J. Phys. Soc. Jpn.* **2013**, *82*, 043702.
(9) Sim, H.; Cheong, S. W.; Kim, B. G. *Phys. Rev. B* **2013**, *88*, 014101.
(10) Zamkova, N. G.; Zhandun, V. S.; Zinenko, V. I. *Phys. Status Solidi B* **2013**, *250*, 1888−1897.
(11) Schaak, R. E.; Mallouk, T. E. *Chem. Mater.* **2002**, *14*, 1455−1471.
(12) Zener, C. *Phys. Rev.* **1951**, *81*, 440−444.
(13) (a) Flem, G. L.; Demazeau, G.; Hagenmuller, P. *J. Solid State Chem.* **1982**, *44*, 82−88. (b) Rao, C.; Ganguly, P.; Singh, K.; Ram, R. *J. Solid State Chem.* **1988**, *72*, 14−23.
(14) (a) Greenblatt, M. *Curr. Opin. Solid State Mater. Sci.* **1997**, *2*, 174−183. (b) Singh, D. J. *Phys. Rev. B* **1995**, *52*, 1358−1361.
(15) In $(ABO_3)_n/(AO)$ RP phases, NCS structures are favored in n = even family of compounds that have two symmetrically inequivalent AO layers as suggested in ref 56.
(16) Birol, T.; Benedek, N. A.; Fennie, C. J. *Phys. Rev. Lett.* **2011**, *107*, 257602.
(17) Fennie, C. J.; Rabe, K. M. *Phys. Rev. B* **2005**, *71*, 100102.
(18) Rodgers, J. A.; Battle, P. D.; Dupré, N.; Grey, C. P.; Sloan, J. *Chem. Mater.* **2004**, *16*, 4257−4266.
(19) Autret, C.; Martin, C.; Hervieu, M.; Retoux, R.; Raveau, B.; André, G.; Bourée, F. *J. Solid State Chem.* **2004**, *177*, 2044−2052.
(20) (a) Leonowicz, M.; Poeppelmeier, K.; Longo, J. *J. Solid State Chem.* **1985**, *59*, 71−80. (b) Matar, S.; Subramanian, M.; Weihrich, R. *Chem. Phys.* **2005**, *310*, 231−238. (c) Wei, Z.; Pei-Qing, T. *Chin. Phys. B* **2013**, *22*, 066201.
(21) Ascher, E.; Kobayashi, J. *J. Phys. C: Solid State Phys.* **1977**, *10*, 1349.
(22) Hatch, D. M.; Stokes, H. T. *Phys. Rev. B* **2001**, *65*, 014113.
(23) (a) Hatch, D. M.; Stokes, H. T.; Aleksandrov, K. S.; Misyul, S. V. *Phys. Rev. B* **1989**, *39*, 9282−9288. (b) Aleksandrov, K. S.; Beznosikov, B. V.; Misyul, S. V. *Phys. Status Solidi A* **1987**, *104*, 529−543. (c) Harris, A. B. *Phys. Rev. B* **2012**, *85*, 174107.
(24) Howard, C. J.; Stokes, H. T. *Acta Crystallogr., Sect. B* **1998**, *54*, 782−789.
(25) (a) Campbell, B. J.; Stokes, H. T.; Tanner, D. E.; Hatch, D. M. *J. Appl. Crystallogr.* **2006**, *39*, 607−614. (b) Orobengoa, D.; Capillas, C.; Aroyo, M. I.; Pérez-Mato, J. M. *J. Appl. Crystallogr.* **2009**, *42*, 820−833. (c) Howard, C. J.; Carpenter, M. A. *Acta Crystallogr., Sect. B* **2012**, *68*, 209−212. (d) Talanov, V. M.; Shirokov, V. B. *Acta Crystallogr., Sect. A* **2012**, *68*, 595−606.
(26) Stokes, H.; Hatch, D.; Campbell, B. J. *ISOTROPY Software Suite*, 2007; http://stokes.byu.edu/iso/isotropy.php.
(27) Miller, S. C.; Love, W. F. *Tables and Irreducible Representations of Space Groups and Co-representations of Magnetic Space Group*; Pruett Press: Boulder, CO, 1967.
(28) Stokes, H. T.; Campbell, B. J.; Cordes, R. *Acta Crystallogr., Sect. A* **2013**, *69*, 388−395.
(29) Kresse, G.; Furthmüller, G. *Comput. Mater. Sci.* **1996**, *6*, 15−50.
(30) Kresse, G.; Joubert, D. *Phys. Rev. B* **1999**, *59*, 1758−1775.
(31) Perdew, J. P.; Ruzsinszky, A.; Csonka, G. I.; Vydrov, O. A.; Scuseria, G. E.; Constantin, L. A.; Zhou, X.; Burke, K. *Phys. Rev. Lett.* **2008**, *100*, 136406.
(32) Monkhorst, H. J.; Pack, J. D. *Phys. Rev. B* **1976**, *13*, 5188−5192.
(33) Our preliminary calculations reveal that the addition of on-site correlations on the Ir 5*d* states using a "plus Hubarrd *U*" correction does not qualitatively change our results; it enhances the rotational distortion amplitudes and reduces the difference between competing phases.
(34) (a) Miao, M.-S.; Seshadri, R. *J. Phys.: Condens. Matter* **2012**, *24*, 215503. (b) Kim, B. J.; Jin, H.; Moon, S. J.; Kim, J.-Y.; Park, B.-G.; Leem, C. S.; Yu, J.; Noh, T. W.; Kim, C.; Oh, S.-J.; Park, J.-H.; Durairaj, V.; Cao, G.; Rotenberg, E. *Phys. Rev. Lett.* **2008**, *101*, 076402. (c) Zeb, M. A.; Kee, H.-Y. *Phys. Rev. B* **2012**, *86*, 085149.
(35) Brock, C. P.; Dunitz, J. D. *Chem. Mater.* **1994**, *6*, 1118−1127.
(36) Patel, R.; Simon, C.; Weller, M. T. *J. Solid State Chem.* **2007**, *180*, 349−359.
(37) Millburn, J.; Green, M.; Neumann, D.; Rosseinsky, M. *J. Solid State Chem.* **1999**, *145*, 401−420.
(38) Toda, K.; Kameo, Y.; Kurita, S.; Sato, M. *J. Alloys Compd.* **1996**, *234*, 19−25.
(39) Schaak, R. E.; Mallouk, T. E. *J. Solid State Chem.* **2001**, *161*, 225−232.
(40) Benedek, N. A.; Fennie, C. J. *Phys. Rev. Lett.* **2011**, *106*, 107204.
(41) (a) Nelson-Cheeseman, B. B.; Shah, A. B.; Santos, T. S.; Bader, S. D.; Zuo, J.-M.; Bhattacharya, A. *Appl. Phys. Lett.* **2011**, *98*, 072505. (b) Yan, L.; Niu, H. J.; Duong, G. V.; Suchomel, M. R.; Bacsa, J.; Chalker, P. R.; Hadermann, J.; van Tendeloo, G.; Rosseinsky, M. J. *Chem. Sci.* **2011**, *2*, 261−272.
(42) (a) Krushke, J. K. *Doing Bayesian Data Analysis*; Academic Press, Elsevier: Oxford, UK, 2011; (b) Efron, B. *Science* **2013**, *340*, 1177−1178.
(43) R Core Team. *R: A Language and Environment for Statistical Computing*; R Foundation for Statistical Computing: Vienna, Austria, 2012; ISBN 3-900051-07-0.
(44) Cheng, J.; Greiner, R. In *Advances in Artificial Intelligence*; Stroulia, E., Matwin, S., Eds.; Lecture Notes in Computer Science; Springer: Berlin Heidelberg, 2001; Vol. *2056*, pp 141−151.
(45) Svetnik, V.; Liaw, A.; Tong, C.; Culberson, J. C.; Sheridan, R. P.; Feuston, B. P. *J. Chem. Inf. Comput. Sci.* **2003**, *43*, 1947−1958 PMID: 14632445..
(46) Noble, W. S. *Nat. Biotechnol.* **2006**, *24*, 1564.
(47) Balachandran, P. V.; Broderick, S. R.; Rajan, K. *Proc. R. Soc. A: Math., Phys. Eng. Sci.* **2011**, *467*, 2271−2290.
(48) Okabe, H.; Isobe, M.; Takayama-Muromachi, E.; Koda, A.; Takeshita, S.; Hiraishi, M.; Miyazaki, M.; Kadono, R.; Miyake, Y.; Akimitsu, J. *Phys. Rev. B* **2011**, *83*, 155118.
(49) Although Ba_2IrO_4 is commonly regarded as an antiferromagnetic insulator with undistorted *I*4/*mmm* structure,[57] we note that there are no lattice dynamical calculations aimed at resolving the ground state structure for this system in the literature. Our work reveal the presence of an antiferrodistortive "soft mode" at the zone boundary (P) of the Brillouin zone.
(50) (a) Crawford, M. K.; Subramanian, M. A.; Harlow, R. L.; Fernandez-Baca, J. A.; Wang, Z. R.; Johnston, D. C. *Phys. Rev. B* **1994**, *49*, 9198−9201. (b) Cosio-Castaneda, C.; Tavizon, G.; Baeza, A.; de la Mora, P.; Escudero, R. *J. Phys.: Condens. Matter* **2007**, *19*, 446210.
(51) Babel, D.; Rüdorff, W.; Tschöpp, R. *Z. Anorg. Allg. Chem.* **1966**, *347*, 282−288.
(52) Kim, B. J.; Ohsumi, H.; Komesu, T.; Sakai, S.; Morita, T.; Takagi, H.; Arima, T. *Science* **2009**, *323*, 1329−1332.
(53) To conclusively determine the set of coupled modes that may form the primary order parameter requires an evaluation of the modes' contributions to the energetic stability of the distorted phase, i.e., using a method with access to total energies. Thus, it is beyond the capability of group theory alone. Note that, on the basis of symmetry arguments, $X_2^+ \oplus M_5^+$ or $X_3^+ \oplus M_5^+$ could be the primary set, although the contribution of M_5^+ to the ground state is smaller than that of X_2^+ or X_3^+.
(54) (a) Fong, D. D.; Stephenson, G. B.; Streiffer, S. K.; Eastman, J. A.; Auciello, O.; Fuoss, P. H.; Thompson, C. *Science* **2004**, *304*, 1650−1653. (b) Borisevich, A. Y.; Chang, H. J.; Huijben, M.; Oxley, M. P.; Okamoto, S.; Niranjan, M. K.; Burton, J. D.; Tsymbal, E. Y.; Chu, Y. H.; Yu, P.; Ramesh, R.; Kalinin, S. V.; Pennycook, S. J. *Phys. Rev. Lett.* **2010**, *105*, 087204. (c) Rondinelli, J. M.; May, S. J.; Freeland, J. W. *MRS Bull.* **2013**, *37*, 261−270. (d) Kim, Y.-M.; Kumar, A.; Hatt, A.; Morozovska, A. N.; Tselev, A.; Biegalski, M. D.; Ivanov, I.; Eliseev, E. A.; Pennycook, S. J.; Rondinelli, J. M.; Kalinin, S. V.; Borisevich, A. Y. *Adv. Mater.* **2012**, *25*, 2497−2504.
(55) (a) Haeni, J. H.; Theis, C. D.; Schlom, D. G.; Tian, W.; Pan, X. Q.; Chang, H.; Takeuchi, I.; Xiang, X.-D. *Appl. Phys. Lett.* **2001**, *78*, 3292−3294. (b) Graboy, I. E.; Bosak, A. A.; Gorbenko, O. Y.; Kaul, A.

R.; Dubourdieu, C.; Sénateur, J.-P.; Svetchnikov, V. L.; Zandbergen, H. W. *Chem. Mater.* **2003**, *15*, 2632−2637. (c) Kozuka, Y.; Seki, H.; Fujita, T. C.; Chakraverty, S.; Yoshimatsu, K.; Kumigashira, H.; Oshima, M.; Bahramy, M. S.; Arita, R.; Kawasaki, M. *Chem. Mater.* **2012**, *24*, 3746−3750.
(56) Benedek, N. A.; Mulder, A. T.; Fennie, C. J. *J. Solid State Chem.* **2012**, *195*, 11−20.
(57) Moser, S.; Moreschini, L.; Ebrahimi, A.; Piazza, B. D.; Isobe, M.; Okabe, H.; Akimitsu, J.; Mazurenko, V.; Kim, K.; Bostwick, A.; Rotenberg, E.; Chang, J.; Rønnow, H.; Grioni, M. *ArXiv e-prints* **2013**, 1−13 Article ID: 1310.1307.